Influence of Spatial Structures on the Resistive Switching Behaviors of Novel Polyimides Containing Tetraphenyl-9H Fluorene Moiety

Lunjun QU(瞿伦君), Yanren ZHENG, Yi ZHANG*(张艺), Zhenguo CHI, Siwei LIU, Jiarui XU

PCFM Lab, GD HPPC Lab, Guangdong Engineering Technology Research Centre for High-performance Organic and Polymer Photoelectric Functional Films, State Key Laboratory of Optoelectronic Materials and Technologies, School of Chemistry and Chemical Engineering, Sun Yat-sen University(中山大学), Guangzhou 510275, China, E-mail:ceszy@mail.sysu.edu.cn

Abstract: Two novel diamines 4,4'-(9,9-diphenyl-9H-fluorene-2,7-diyl)dianiline (TPF-2,7-DA) and 4,4'-(2,7-diphenyl-9H-fluorene-9,9-diyl)dianiline (TPF-9,9-DA) were designed and synthesized based on tetraphenyl-9H-fluorene, and the novel polyimides (PIs), PI (TPF-2,7-DA-ODPA) and PI(TPF-9,9-DA-ODPA) were prepared with the diamines and 4,4'-Oxydiphthalic dianhydride (ODPA). The device with the structure of ITO/PI (TPF-2,7-DA-ODPA) /Al was found to show "write once, read many times" (WORM) switching behavior, while the device of ITO/PI (TPF-9,9-DA-ODPA) /Al exhibited "static random access memory" (SRAM) switching behavior.

Key Words: polyimide; tetraphenyl-9H-fluorene; spatial structures; resistive switching behaviors

Over the past decade, polyimide (PI) materials were applied to resistive memory device researches mainly because of their excellent thermal stability, chemical stability and mechanical properties. Compared to inorganic semiconductor materials, the organic polymer materials were easy processing, flexibility, low cost, etc. Thus, polyimide materials were considered to be used for the next generation electrical resistive memory applications.

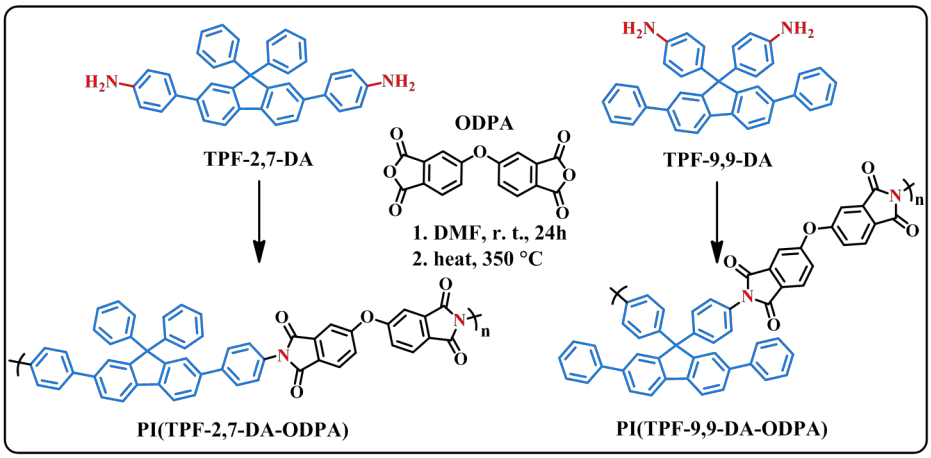

Scheme 1. Synthetic route for PI (TPF-2,7-DA-ODPA) and PI (TPF-9,9-DA-ODPA).

Although various functional polyimides have been investigated for the applications in the fields of memory devices, there were few studies to explore the influence of spatial structures of polyimides on the resistive switching behaviors in PIs-based memory devices. In this work, we reported two novel diamines 4,4'-(9,9-diphenyl-9H-fluorene-2,7-diyl)dianiline (TPF-2,7-DA) and 4,4'-(2,7-diphenyl-9H-fluorene-9,9-diyl)dianiline (TPF-9,9-DA) with similar chemical composition and molecular weight, but the polyimides, PI (TPF-2,7-DA-ODPA) and PI (TPF-9,9-DA-ODPA) were completely different in the spatial structure of the chemical structure units, as shown **Scheme 1**. The resistive switching

behaviors, conducted by a simple sandwich device configuration consisting of a spin-coated PIs films between ITO bottom electrode and Al top electrode, were also different. The device of the configuration of ITO/PI (TPF-2,7-DA-ODPA) /Al showed "write once, read many times"(WORM) switching behavior, while the device of ITO/PI (TPF-9,9-DA-ODPA) /Al exhibited "static random access memory" (SRAM) switching behavior. In order to clarify the switching mechanism of the devices, theoretical calculations under the density functional theory (DFT) method at the B3LYP level with the 6-31G (d) basic set, were applied to analyze the geometry and electronic transitions of the studied polyimides. This study suggested that the electrical resistive switching performances could be turned through the careful design of the spatial structures of the polyimides.

The UV-vis. absorption spectra of the polyimides in DMF solutions (~$1*10^{-5}$ M) and the cyclic voltammetry (CV) of the PI films on the ITO glasses using 0.1 M solution of tetrabutylammonium perchlorate (TBAP) in anhydrous acetonitrile were summarized in **Table 1**. PI (TPF-2,7-DA-ODPA) exhibited an initial absorption ($\lambda_{abs\ onset}$) and a maximum absorption ($\lambda_{abs\ max}$) peak at around 377 nm and 340 nm in solution, while those of PI (TPF-9,9-DA-ODPA) were around 362 nm and 333 nm respectively. The above absorption peaks were attributed to the π-π^* transition delocalized along the π-electronic system. The optical band gaps (E_g) of PI (TPF-2,7-DA-ODPA) and PI (TPF-9,9-DA-ODPA), determined from the onset optical absorbance, were 3.29 eV and 3.43 eV respectively. Thus, the estimated highest occupied molecular orbital (HOMO) level of PI (TPF-2,7-DA-ODPA) and PI (TPF-9,9-DA-ODPA) were -5.05 eV and -5.02 eV, the lowest occupied molecular orbital (LUMO) level of PIs estimated from the difference between the optical band gap (E_g) and HOMO energy were -1.76 eV and -1.59 eV respectively.

Table 1. Optical and electrochemical properties of the Polyimides.

Polyimides	In solution [a] (nm)		Oxidation Voltage [b] (V)	E_g [c] (eV)	HOMO [d] (eV)	LUMO [e] (eV)	HOMO [f] (eV)	LUMO [f] (eV)
	$\lambda_{abs\ onset}$	$\lambda_{abs\ max}$	*Eox onset*					
TPF-2,7-DA-ODPA	377	340	0.63	3.29	-5.05	-1.76	-5.42	-5.44
TPF-9,9-DA-ODPA	362	333	0.60	3.43	-5.02	-1.59	-2.51	-2.44

[a] Measured in dilute solution in DMF (~$1*10^{-5}$ M).

[b] Obtained from cyclic voltammetry versus Ag/AgCl in CH_3CN.

[c] $E_g = 1240/\lambda_{onset}$ eV.

[d] $E_{HOMO} = -[E_{onset}^{ox} - E(Fc/Fc^+)+4.8]$ eV, the HOMO energy level was calculated from cyclic voltammetry and referenced to ferrocene (4.8 eV).

[e] $E_{LUMO} = E_{HOMO} + E_g$.

[f] Basic unit of PI was calculated by DFT/B3LYP/6-31G(d) with the Gaussian 09 program.

The resistive switching behaviors effects of PI (TPF-2,7-DA-ODPA) and PI (TPF-9,9-DA-ODPA) were conducted by the current-voltage (*I-V*) characteristics of the ITO/PI/Al devices (as shown in **Figure 1 (a)**). The resistive switching characteristics of the devices based on the high conductivity (ON) and the low conductivity (OFF) response to the external applied voltages. **Figure 1 (b)** and **(c)**

exhibited the typical *I-V* curves of the ITO/PI (TPF-2,7-DA-ODPA) /Al and ITO/PI (TPF-9,9-DA-ODPA) /Al devices (recorded device units of 0.5*0.5 mm^2) at a scan rate of 0.05 V/s. The thickness of polyimide layer was estimated to be around 60 nm. For the case of ITO/PI (TPF-2,7-DA-ODPA) /Al device, as the voltage first sweep from 0 to 5 V, the device was initially in the OFF state ("0" signal in memory data storage) with a current in the range of 10^{-12}~10^{-9} A. However, the continuous sweeping induced an abrupt increase in current around 1.7 V, which was defined as the switching threshold voltage. The ON/OFF current ratio was roughly as high as 10^4. This electronic transition from the OFF state to ON state in the first sweep served as the "writing" progress ("1" signal in memory data storage). In addition, the device could be kept in the ON state during the subsequent second sweep from 5 to 0 V. The nest dual sweeps (third and fourth sweep) were performed after turning the power off for usually less than 3 minutes, the ON state could also be kept, indicating that the device was non-erasable. The long retention ability of the ON state determined the WORM functionality of the ITO/PI (TPF-2,7-DA-ODPA) /Al device.

For the case of ITO/PI (TPF-9,9-DA-ODPA) /Al device, the first and second sweep were similar with ITO/PI (TPF-2,7-DA-ODPA) /Al device except that the abrupt increase in current was around 2.0V at the first sweep. The third sweep was conducted after turning off the power for about 3 minutes. The device could be reprogrammed, starting from the OFF state, to the ON state again with an accurate threshold voltage at -2.0 V and kept the ON state (the third and the fourth sweeps). It suggested that the ON state could be retained for a short period of time after the removal of power and would relax to the original OFF state eventually. Therefore, the switching behavior could be explained the SRAM functionality.

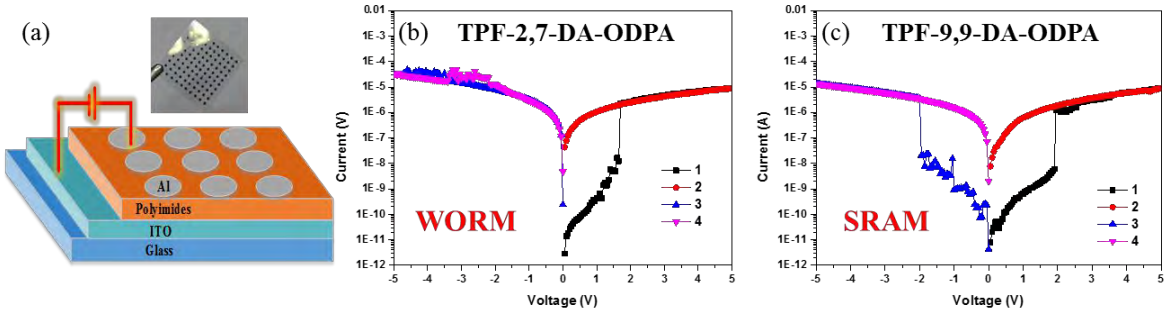

Figure 1. (a) Image and schematic diagram of the electronic device; (b) and (c) current-voltage (*I-V*) characteristic curves of ITO/PI (TPF-2,7-DA-ODPA) and (TPF-9,9-DA-ODPA) /Al electronic device.

Molecular simulations on the basic unit of PI (TPF-2,7-DA-ODPA) and PI (TPF-9,9-DA-ODPA), were carried out by the DFT/B3LYP.6-31 G (d) with the Gaussian 09 program. The sketch map of the structures for the basic unit of PI and optimized structures were plotted to the right of **Figure 2**. The molecule of the tetraphenyl-9H-fluorene in the basic unit was totally non-planar, and the twisted conformation of PI (TPF-2,7-DA-ODPA) and PI (TPF-9,9-DA-ODPA) were contributed from the non-planar geometry between the tetraphenyl-9H-fluorene and imide ring unit (37°, 40° and 42°, 145°respectively).

The left part of **Figure 2** showed the charge density isosurfaces of the basic unit of PI (TPF-2,7-DA-ODPA) and PI (TPF-9,9-DA-ODPA) with the most energetically favorable geometry. The relative ordering of the occupied and virtual molecular orbitals gave a reasonable indication of the excited properties and charge-transport (CT) ability. Both the HOMO and the LUMO+4 isosurfaces tended to lacatd on TPF-2,7-DA or TPF-9,9-DA (donor), while the LUMO and the LUMO+1 located

on ODPA (acceptor). The distributed surfaces showed that the HOMO in basic unit of PI (TPF-2,7-DA-ODPA) and PI (TPF-9,9-DA-ODPA) might interact with the LUMO for CT formation. The electron localization in the HOMO revealed the low OFF state current (10^{-12}~10^{-9} A). Due to the influence of the spatial structures between tetraphenyl-9H-fluorene and imide ring unit, the LUMO+2 and LUMO+3 located mainly on the TPF-2,7-DA and partly on the ODPA, while the LUMO+2 and the LUMO+3 located only on the TPF-2,7-DA.

For the case of PI (TPF-2,7-DA-ODPA), as the applied bias at threshold voltage, electro at the HOMO with sufficient energy transited to the LUMO+2, the LUMO+3 and the LUMO+4 within donors units to give rise to excited state. CT could be observed form the conductive complex through processes such as indirectly from the LUMO+2 to the LUMO+1and then to the LUMO. While for the case of PI (TPF-9,9-DA-ODPA), CT could be observed from the LUMO+4 to the LUMO+3, to the LUMO+2, to the LUMO+1 and then to the LUMO. This indicated that the excitation energy of PI (TPF-9,9-DA-ODPA) was higher than that of PI (TPF-2,7-DA-ODPA), which was in compliance with the threshold voltage (2.0 V >1.7 V). Meanwhile, the high excitation energy might lead the unstable CT state and rapidly return to the original OFF state. Therefore, the large twisted spatial structure of PI (TPF-9,9-DA-ODPA) would lead to the unstable CT state, and then lead to show SRAM switching behavior. On the contrary, PI (TPF-2,7-DA-ODPA) tended to show WORM switching behavior.

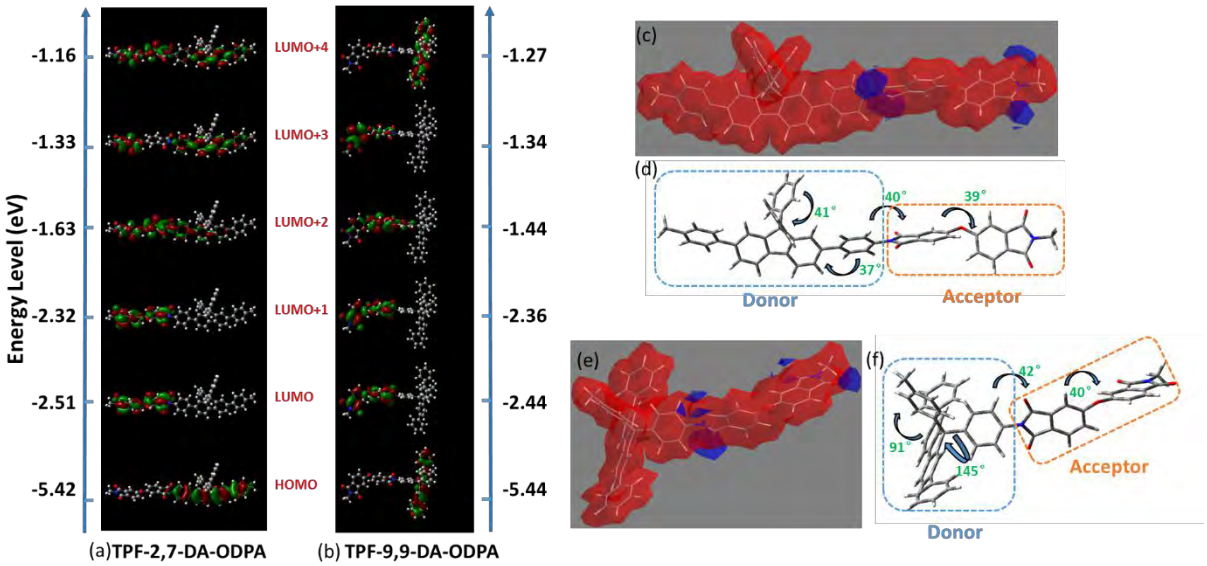

Figure 2. Optimized geometries and electric density contours for molecular orbitals of (a) PI (TPF-2,7-DA-ODPA) and (b) PI (TPF-9,9-DA-ODPA); Electrostatic potential of the basic unit of (c) PI (TPF-2,7-DA-ODPA) and (e) PI (TPF-9,9-DA-ODPA) ; Optimized geometries of the basic unit of (d) PI (TPF-2,7-DA-ODPA) and (f) PI (TPF-9,9-DA-ODPA).

In summary, we have successfully synthesized new polyimides consisting of tetraphenyl-9H-fluorene (electron donor) and dianhydride (electron acceptor) for electrical resistive memory applications. Due to the twisted spatial structure of PI tending to lead to unstable CT state, resistive switching behaviors of the PIs-based memory devices would be also different. The present study provided a new insight on switching characteristics for advanced memory device applications.

The financial support by the National 973 Program of China (No. 2014CB643605), the National

863 Program of China (No. 2015AA033408), the National Natural Science Foundation of China (Nos. 51373204, 51233008, and J1103305), the Science and Technology Project of Guangdong Province (Nos. 2015B090915003 and 2015B090913003), the Doctoral Fund of the Ministry of Education of China (No. 20120171130001), and the Fundamental Research Funds for the Central Universities (No. 161gzd08) are gratefully acknowledged.

Reference

[1]. Z. X. Zhou, L. J. Qu, T. T. Yang, J. L. Wen, Y. Zhang, Z. G. Chi, S. W. Liu, X. D. Chen and J. R. Xu, *RSC Adv.*, **2016**, 6, 52798-52809.

[2]. Liu, Y. W.; Zhang, Y.; Lan, Q.; Qin, Z. X.; Liu, S. W.; Zhao, C. Y.; Chi, Z. G.; Xu, J. R. Synthesis and properties of high-performance functional polyimides containing rigid nonplanar conjugated tetraphenylethylene moieties. *Chem. Mater.*, **2012**, 24, 1212−1222.

(continued from p60)

[3] Bang A., Buback C. Sotiriou-Leventis C., Leventis N. Chemistry of Materials, 26, 6979−6993 (2014).

[4] Meador M-A-B., Malow E-J., Silva R., Wright S., Quade D., Vivod S-L., Guo H-Q., Guo J., Cakmak M. ACS Applied Material Interfaces, **4**, 536-544 (2012).

[5] Guo H-Q., Meador M-A-B., McCorkle L, Quade D-J., Guo J., Hamilton B., Cakmak M., Sprowl G. ACS Applied Material Interfaces, **3**, 546-552 (2011).

[6] Meador M-A-B., Aleman C-R., Hanson K., Ramirez N., Vivod S-L., Wilmoth N., McCorkle L. ACS Applied Material Interfaces, **7**, 1240-1249 (2015).

[7] Pei X-L., Zhai W-T., Zheng W-G. Langmuir, 30, 13375-13383 (2014).

[8] Meador M-A-B., Wright S., Sandberg A., Nguyen B. N., Keuls F-W-V., Mueller C-H., Rodriguez-Solis R., Miranda F-A. ACS Applied Material Interfaces, **4**, 6346-6353 (2012).

[9] Meador M-A-B., McMillon E., Sandberg A., Barrios E., Wilmoth N-G., Mueller C-H., Miranda F-A. ACS Applied Materials&Interfaces, **6**, 6062-6068 (2014).

[10] Shen D-X., Liu J-G., Yang H-X., Yang S-Y. Chemistry Letters, **42**,1230-1232 (2013).

[11] Fukukawa K., Shibasaki Y., Ueda M. Macromolecules, **37**, 8256-8261 (2004).

[12] Aegerter M-A., Leventis N., Koebel M-M.: Aerogel Handbook, Springer, New York (2011).

[13] Li L-C., Yalcin B., Nguyen B-N., Meador M-A-B., Cakmak M. ACS Applied Materials&Interfaces, **1**, 2491-2501 (2009).

[14] Hrubesh L-W., Pekala R-W.: Dielectric properties and electronic applications of aerogels. in 'Sol-Gel Processing and Applications' (ed.: Attia Y-A.) Plenum Press, New York, 363-367 (1994).